Weather and Climate Extremes 49 (2025) 100796

Contents lists available at ScienceDirect

Weather and Climate Extremes

journal homepage: www.elsevier.com/locate/wace

Multi-task feature transfer deep learning-based tropical cyclone center estimation (MFT–TC) using geostationary satellite observations

Juhyun Lee [a,b], Il-Ju Moon [c,*], Jungho Im [a,d,e,**], Dong-Hoon Kim [c], Hyeyoon Jung [c]

[a] Department of Civil, Urban, Earth, & Environmental Engineering, Ulsan National Institute of Science and Technology (UNIST), Ulsan, Republic of Korea
[b] Department of Atmospheric Science, Colorado State University, CO, USA
[c] Typhoon Research Center, Jeju National University, Jeju, Republic of Korea
[d] Gradudate School of Artificial Intelligence, UNIST, Ulsan, Republic of Korea
[e] Graduate School of Carbon Neutrality, UNIST, Ulsan, Republic of Korea

ARTICLE INFO

Keywords:
Typhoon center determination
Novel deep learning
Explainable AI

ABSTRACT

Accurate and rapid tropical cyclone (TC) monitoring is crucial for precise forecasting and appropriate response to mitigate socio-economic damages. Geostationary satellite-based observations are the only tools that allow continuous monitoring of TCs throughout their entire lifetime, from formation to dissipation. However, owing to the diversity of TC structures, the automatic extraction of TC information using geostationary satellite-based cloud-top observations is still challenging. To address this limitation, several deep-learning-based approaches for extracting TC information have been developed. Here, we propose a novel deep learning-based TC center estimation approach using real-time geostationary satellite observations. To reduce computational costs while capturing both the entire TC structure and high-resolution spiral patterns, we propose a multi-task feature transfer deep learning-based TC center estimation (MFT–TC). This model effectively considers both the entire spiral band and focuses on specific local characteristics of TC while maintaining high computing efficiency, reducing computing costs by 47 %). Compared to the conventional single-CNN-based TC center determination model, which has been widely used in previous studies, the proposed model achieved significant improvements, with skill score increases ranging from 12 % to 39 %. Additionally, since there are significant structural differences between TCs with and without an eye, MFT–TC was evaluated under two different schemes based on the training sets: scheme 1, which uses separate training datasets depending on whether the TC has an eye (MFT–TC-div) and scheme 2, which uses all TC cases combined (MFT–TC-whl). Evaluation results showed scheme 1-based MFT–TC achieved a 14.8 % improvement over scheme 2-based MFT–TC, suggesting that separating training samples based on TC eye presence enhances the accuracy of TC center estimation. Furthermore, using the explainable artificial intelligence (XAI) approach, we demonstrated that MFT–TC efficiently captures both overall cyclonic structures and center-specific spatial characteristics to estimate the TC center accurately.

1. Introduction

Tropical cyclones (TCs) induce critical socioeconomic damage owing to severe winds and heavy rainfall and the uncertainty of predictability has been increased due to climate change (Knapp et al., 2010; Mahapatra et al., 2018; Forbis et al., 2024; Wu et al., 2024). Although monitoring TCs is crucial for enhancing forecasting accuracy and minimizing the resulting damage, instruments to real-time monitor the whole lifetime of a TC are lacking. Geostationary satellites are the sole means of observing TCs during their entire lifecycle, from formation to dissipation. The Dvorak technique (Dvorak, 1975; 1984), a method for analyzing the cyclonic patterns of TCs using geostationary satellite-based infrared channels, has been widely utilized to determine TC centers in operation. However, the operational method has limitations in that it is difficult to exclude the subjectivity of forecasters and requires analysis time to obtain TC information.

To mitigate these limitations, several automatic TC center estimation methods using geostationary satellites have been proposed, which are

* Corresponding author. Typhoon Research Center, Jeju National University, Jeju, Republic of Korea.
** Corresponding author. Department of Civil, Urban, Earth, & Environmental Engineering, Ulsan National Institute of Science and Technology (UNIST), Ulsan, Republic of Korea.
E-mail addresses: ijmoon@jejunu.ac.kr (I.-J. Moon), ersgis@unist.ac.kr (J. Im).

https://doi.org/10.1016/j.wace.2025.100796
Received 3 November 2024; Received in revised form 4 July 2025; Accepted 14 July 2025
Available online 16 July 2025

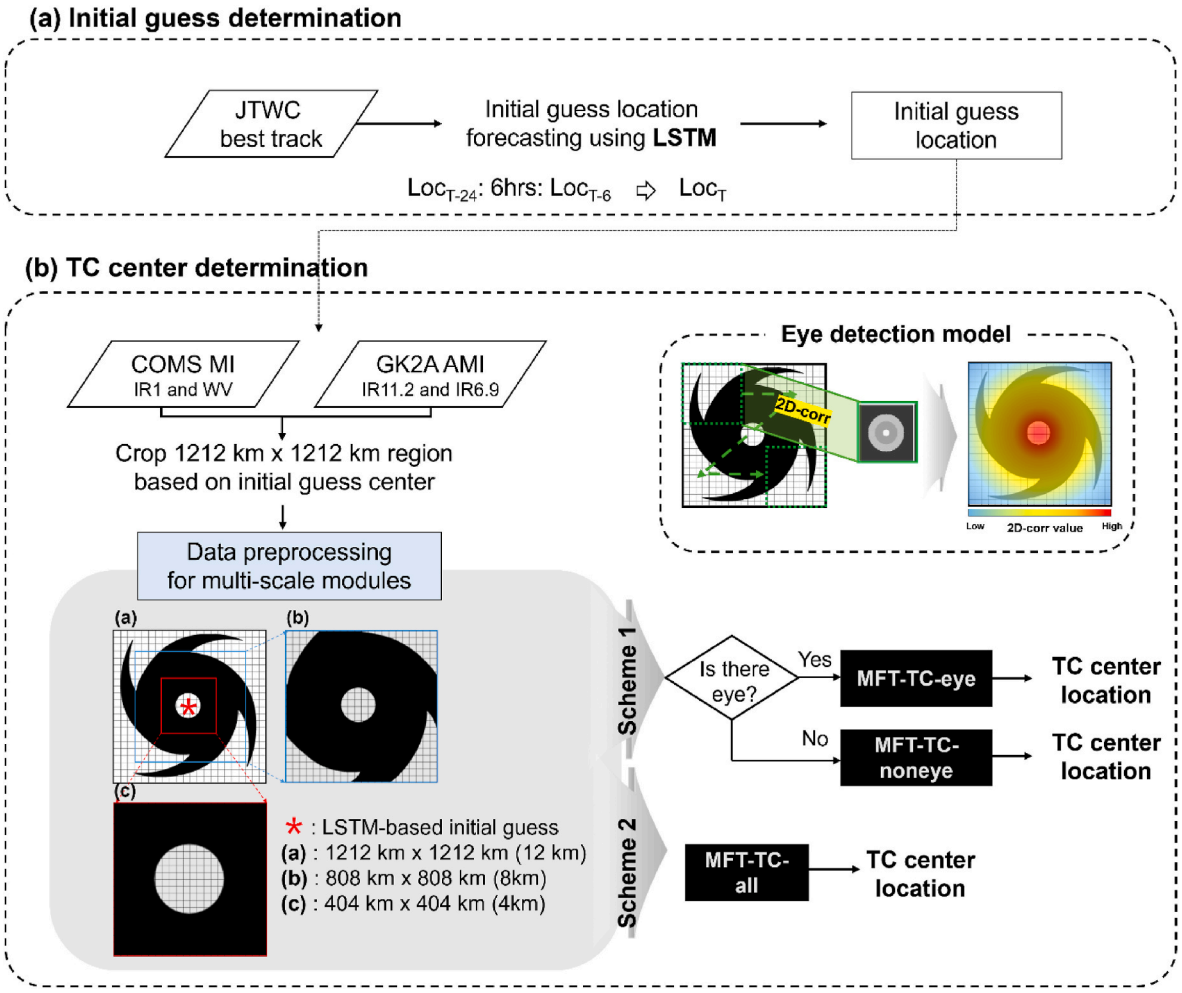

Fig. 1. Overall flow of multi-task feature transfer deep learning-based TC center estimation (MFT–TC) approach. It consists of two automatic steps—initial guess determination and TC center determination—and includes two schemes for estimating the TC center.

divided into two approaches: 1) statistical methods and 2) deep learning-based methods. For statistical approaches, some methods utilize the gradient of brightness temperatures (BTs) around the TC system (e.g., Zheng et al., 2019; Hu et al., 2021) or consider highly convective cyclonic patterns around the TC center (e.g., Lu et al., 2019; Shin et al., 2022). Assuming a highly convective region in the low-BT pixels in long-wave infrared (IR) channel-based observations, the former considers the gradient of BTs around neighboring pixels and finds that the highest concentrated region is the TC center. In contrast, the latter considers the intensity-wise most convective spiral band region around the TC center and identifies the most fitted region as the TC center. These statistical approaches are advantageous in terms of providing intuitive knowledge of how the center was determined. However, they tend to optimize for ideal TC cases, and limitations exist in improving the performance of outlier cases.

As an alternative, several deep-learning-based TC center estimation approaches have been proposed (e.g., Ho et al., 2024; Wang et al., 2024; Zhang et al., 2024). These approaches widely use convolutional neural networks (CNNs) to determine the center locations from satellite-based TC observations. They efficiently considered the horizontal pattern of TCs for determining centers by analyzing not only center-closed regional characteristics but also the outflows of TCs. This mitigates the limitations of statistical approaches. However, it inevitably requires that the input datasets combine entire TC systems to analyze the location of the TC centers. That is, as the spatial resolution of geostationary satellite observations improves, the size of the input datasets inevitably increases, leading to a high computational capacity. When the size of the input dataset increases, the number of parameters required to train the neural networks for optimization rises exponentially. Several studies (e.g., Shin et al., 2022; Wu et al., 2023; Ho et al., 2024) have demonstrated that the performance of automatic TC center determination gets worse as the TC gets weaker, implying that center determination is hard when the TC structure is not ideal. Therefore, it is curial that both of specific characteristics of central region and synoptic structural characteristics of whole TC system should be considered simultaneously.

In this study, a multi-task feature transfer deep learning (MFT) model for TC center estimation is proposed to mitigate the exponentially increasing computing cost while considering the entire TC structure. The model consists of three CNN-based modules, all of which have the same input dataset size. The first module analyzes the entire horizontal TC structure using a low spatial resolution; the second module focuses on the inner region of the TC, employing a medium spatial resolution; the last module concentrates on centrally focused observations utilizing the highest spatial resolution. In this model, the features of the upper module are transferred to the bottom module to transport knowledge of the surrounding spatial patterns, which enables them to interconnect with each other in the entire network. The proposed approach was conducted using two schemes: 1) training all TC cases and 2) dividing them into two TC cases based on whether they contain eyes. Through quantitative evaluation of each scheme, the most optimal approach would be proposed. Furthermore, using heat map, which is one of the explainable AI (XAI) approaches, we qualitatively verified how the

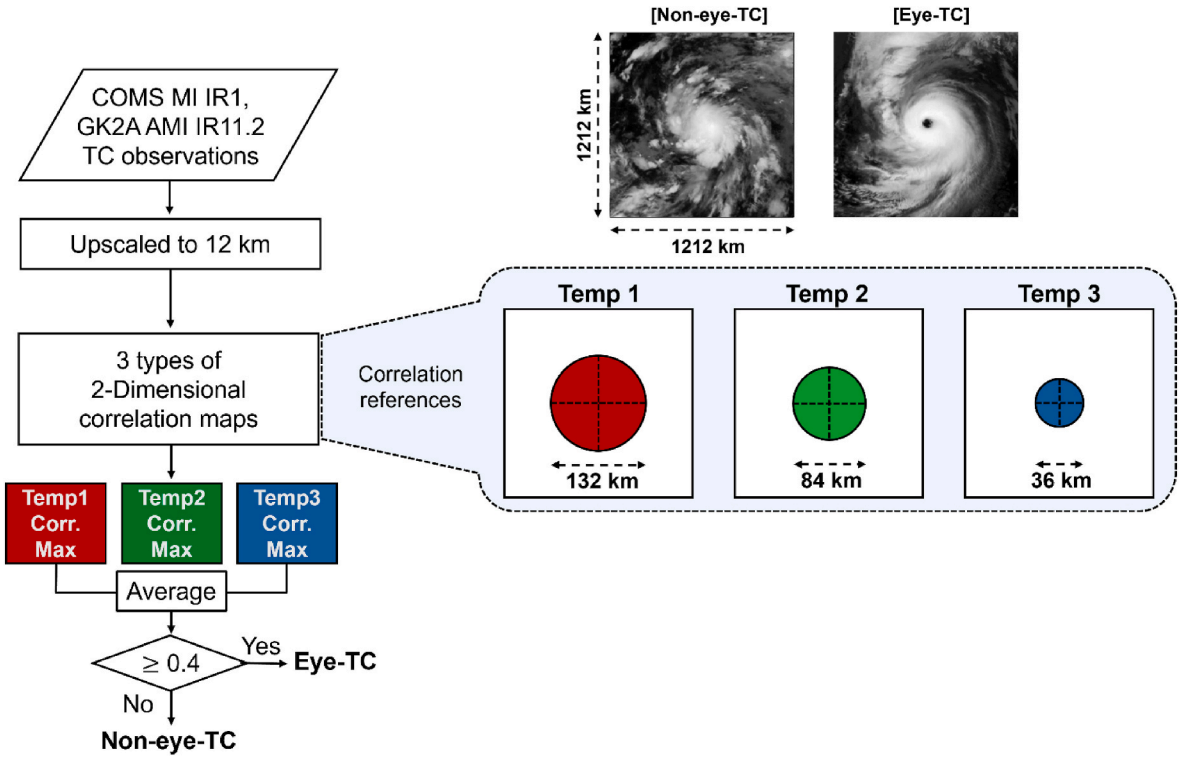

Fig. 2. Statistical template-based eye detection method. TC eye existence is determined through analyzing two-dimensional correlation coefficient using three round templates with 132, 84, and 36 km of size. If the average of maximum values from three template-based correlation maps over the TC observations was over 0.4, the target TC was determined as eye-contained TC.

proposed model works for determining TC center region in the model. Also, we suggested the efficiency of proposed model through comparing with single-CNN-based TC center estimation model, which widely used in the previous studies.

2. Data

2.1. Geostationary satellite data

A geostationary satellite operates at the same speed as Earth's rotation, allowing it to remain fixed in position and observe a specific area of Earth's surface in high resolution. The meteorological sensors carried on them commonly cover wavelengths from visible (0.4–0.6 μm) to longwave IR (8.5–13.3 μm) to monitor atmospheric conditions. In particular, longwave IR channels are sensitive to the water vapor (WV) content in the upper atmosphere, and water vapor channels provide mid-level atmospheric information (Chang and Li, 2005; Lee et al., 2019, 2021; Baek et al., 2022; Yin et al., 2022; Choo et al., 2024; Lee et al., 2025). Therefore, the IR channels of geostationary satellites have been widely utilized to monitor the entire lifetime of TCs (Kurniawan et al., 2024; Chang et al., 2020; Liu et al., 2023; Jung et al., 2024). In this study, one IR channel and one WV channel were utilized to consider both the horizontal spatial pattern and the upper-mid altitudinal water vapor concentration of the TCs. In this study, two geostationary satellites which launched from South Korea were utilized: Communication, Ocean, and Meteorological Satellite (COMS) and GEO-KOMPSAT-2A (GK2A). From COMS meteorological imagery (MI), the IR1 channel, which has a central wavelength of 10.8 μm, and the WV channel, which has a central wavelength of 6.75 μm, were utilized over the Western North Pacific (WNP) region from 2011 to 2019. From GK2A advanced meteorological imager (AMI), two channels (IR6.9, 6.95 μm; IR10.5, 10.5 μm) with wavelengths similar to the MI channels (i.e., WV and IR1) collected over the WNP from 2019 to 2022. Since the GK2A is subsequent mission of COMS, the observation range is same, however, spatial and temporal resolution were improved: COMS MI IR1 and WV have spatial resolution of 4 km and temporal resolution of 15 min, while GK2A AMI IR6.9 and IR10.5 have spatial resolution of 2 km and temporal resolution of 10 min. To utilize both simultaneously, the spatial resolution of each dataset was resampled in 12, 8, and 4 km. COMS MI and GK2A AMI data were obtained from the National Meteorological Satellite Center (NMSC, https://nmsc.kma.go.kr/).

2.2. Best track data

TC information is obtained from the best track data produced by the Joint Typhoon Warning Center (JTWC) (Knapp et al., 2010; Magee et al., 2016). The best track includes 6 hourly information on the TC center location, the maximum sustained wind, minimum sea-level pressure, radius to maximum wind (RMW) and so on. For this study, we utilized TC location, intensity (maximum sustained wind speed) data over the WNP from 2011 to 2021 as a reference, and RMW is also leveraged for discussion.

3. Methodology

This study proposes a geostationary satellite-based multi-task feature transfer deep learning method for estimating the center of tropical cyclone (MTF-TC; Fig. 1). The proposed approach consists of two parts: 1) determining the initial guessed location of TC and 2) estimating TC center location. First, the initial guess of TC location is determined using the Long Short-Term Memory (LSTM)-based model. It extracts the expected on-time TC location using past TC locations, which serves as the initial guess for the TC center when extracting on-time TC regions from the geostationary satellite-based IR window and WV channels. Subsequently, using the copped TC regions, MFT-TC is conducted to determine the exact TC center location. Here, two schemes are tested: Scheme 1 for divided dataset whether TC contains eye or not, and Scheme 2 for all-combined datasets. For verifying feasibility of MFT-TC model, the

	Originally extracted TC images	Module 1	Module 2	Module 3
Input dataset Structures	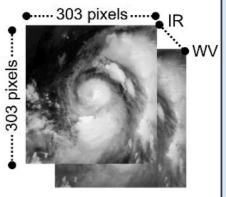	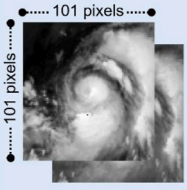	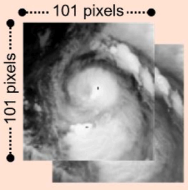	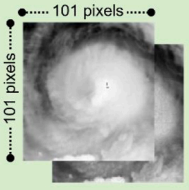
Size	(303 x 303 x 2)	(101 x 101 x 2)	(101 x 101 x 2)	(101 x 101 x 2)
Spatial resolution	4 km	**12 km**	**8 km**	**4 km**

Fig. 3. Input data structures of originally extracted TC images and preprocessed datasets for three modules of multi-task feature transfer deep learning-based tropical center estimation model. Both of infrared window and water vapor channels were utilized and cropped over 1 212 km × 1 212 km area based on long-short term memory LSTM-based initial guess location. Input structures of three modules are same as (101 × 101 x 2) while spatial resolutions were 12, 8, and 4 km.

performance is compared with a single-CNN-based TC center estimation method, which has been widely utilized in previous studies. Furthermore, using heat map, which is one of the explainable AI (XAI) methods, we investigate where each model focused on estimating the TC center location.

3.1. *Initial guess TC location determination using long-short-term memory (LSTM)*

Prior to extracting TC images from satellite observations, an initial estimate of TC location is necessary. There are two ways to obtain an initial guess of TC locations: utilizing numerical model-based forecasting results (e.g., Lu et al., 2019; Lee et al., 2019; Ho et al., 2024) and using estimated results 6 h priorly (e.g., Lee et al., 2019; Wang et al., 2024). Several previous studies (e.g., S. Gao et al., 2018; Lian et al., 2020) have revealed that LSTM is efficient for TC track forecasting, particularly for short-term prediction (i.e., 6 h forecasting). In this study, we utilize a simple LSTM-based TC initial location determination approach to obtain the current TC initial guessed location using hourly time-series location estimation from 24 h to 6 h priorly. LSTM is an advanced model of recurrent neural networks (RNN) leveraged to handle sequential data and long-term dependencies (Hochreiter, 1997; Yu et al., 2019; Jung et al., 2020; Chi, 2022; Hao et al., 2023; Zhu et al., 2024). It can remember and forget the significant information through a specific gating mechanism. One LSTM unit consists of a cell state, hidden state, and four gates (i.e., input gate, forget gate, cell gate, and output gate). We set the TC initial guess estimation model with one LSTM layer facilitating with hidden states of 50 (i.e., the dimension of the hidden state is 50), an activation function of "tanh," and a recurrent activation function of "sigmoid."

3.2. *Eye detection method*

Structural characteristics of TC can be divided in two types: containing eye or not. When the TC has eye, the center of cyclone is clear, however, there is no eye, more wide structural characteristics of the spiral should be considered to determine where is the center of it. Based on this point of view, two schemes are tested according to sample distributions: divided into whether a TC contains an eye or not (Scheme 1) and all samples (Scheme 2). Here, to distinguish the existence of eye, automatic TC eye detection should be prioritized. In this study, we propose a statistical template-based TC eye detection algorithm (ST-eye) (Fig. 2 and Appendix A). The main assumption of ST-eye is that the spatial correlation between the reference round template and TC central region shows higher value when eye exists, compared to non-eye TCs. Since the size of eye varies depending on eye types (i.e., "EYE",

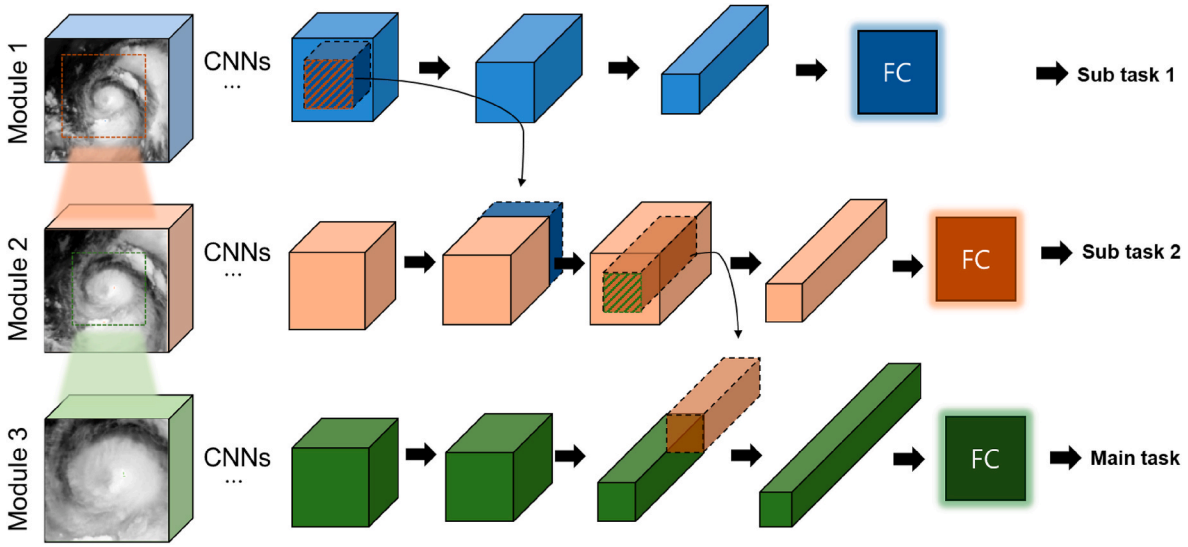

Fig. 4. Overall architecture of multi-task feature transfer deep learning-based TC center estimation model (MFT-TC). Proposed model consists of three modules (i.e., Module 1–3) for considering different scaled TC images (spatial resolution of 12, 8, and 4 km). It makes efficiently considering multi-scaled images for extracting fine resolution characteristics. There are three multi-tasks module, with the main task connected to Module 3 providing the final estimation result.

"PINHOLE", "LARGE") from 5 km to 136 km (Dvorak, 1975, 1984; Velden et al., 1998; Tsukada et al., 2023), three sized circle templates (i.e., *Temp 1–3* with diameters of 132, 84, and 32 km) were utilized for classification. First, each template is adopted and convoluted over IR window (i.e., MI IR1 and AMI IR11.2 channels)-based TC images for calculating 2-dimensional correlation coefficients. Then, an average value of maximum correlation coefficient values from *Temp 1–3* is calculated for determining whether TC contains eye or not. As the average value increases, it can be assumed that the eye-like region is inside the image. Based on statistical analysis (see Appendix A), the threshold for classifying an eye-contain-TC was determined to be 0.4.

3.3. Input data preparation

To develop the TC center estimation models, we first extract satellite images containing TCs from the IR1 (IR11.2) and WV (IR6.9) channels of the COMS MI (GK2A AMI). As TC eyewalls, the shape of spiral rainbands formed by cirrus outflow, and vertical wind shear are crucial structural factors for estimating intensity (Dvorak, 1984), it is necessary to use an image that covers the entire shape of a TC as an input for training the patterns. We delineate the 1 212 × 1 212 km region based on the LSTM-based initial guess center for both the long-wave IR and WV channels. The three types of input datasets are prepared for the MFT–TC model (Fig. 3). In the first module, which encompasses the entire TC structure at low resolution, the cropped image is upscaled to a spatial resolution of 12 km. For the second module, which refers to the internal region of the TC with a medium resolution, the delimited image is enlarged to a resolution of 8 km and cropped to a 101 × 101 pixels area centered around the central pixel. For the final module, a 101 × 101 pixels region is extracted centered around the TC center pixel, and the spatial resolution of each pixel is 4 km. In the proposed MFT–TC model, the three modules (Modules 1, 2, and 3) are interconnected through feature transfer from the upper module to the bottom module.

3.4. Multi-task feature transfer deep learning-based TC center detection model (MFT–TC)

While there are several existing detection methods for multi zoom-in algorithms (e.g., M. Gao et al., 2018; Liu et al., 2021), they detected a specific feature in large-scaled image, and estimated small scaled objects. However, in this study, we proposed the model considering synoptic and local scaled pattern simultaneously, for significantly estimate where the cyclonic center of TC is. We propose a novel algorithm, which is called MFT-TC that merges with the multi-task learning and the feature transfer (FT) deep learning approach (Fig. 4, Table 2). Multi-task learning is a machine learning approach in which a model is trained to extract multiple related tasks (i.e., outputs) simultaneously (Caruana, 1997; Zhang et al., 2018; Lee et al., 2020; Yu et al., 2022). By leveraging similarities between tasks, it enhances performance, especially when data for individual tasks are limited. This is achieved by minimizing a combined loss function, allowing the model to generalize better through shared representations and mutual regularization. It enables the model to learn multiple features simultaneously by utilizing shared representations across different tasks. This allows the model to capture various characteristics within the input dataset. By leveraging similarities between tasks, it enhances performance, especially when data for individual tasks are limited. This is achieved by minimizing a combined loss function, allowing the model to generalize better through shared representations and mutual regularization. In this study, we aim to utilize the advantage of multi-task learning while addressing challenges to handle multi-scaled spatial characteristics and optimize TC center estimation performance. MFT-TC enables sharing the parameters of each module and the spatial characteristics from one module available to effect other module. The model consists of three modules, each corresponding to multi-scale input datasets at resolutions of 12, 8 and 4 km (Fig. 4). Since the input dataset sizes are consistent (i.e., 2 × 101 × 101), receptive areas are varied, with 1 212 km × 1 212 km in Module 1 (the largest-scale module), 808 km × 808 km in Module 2, and 404 km × 404 km in Module 3 (the most focused-scale module). First, the large-scale module is trained to capture the synoptic outflow patterns of the TC in relation to its central location. The centrally focused feature learned in this module is then transferred to the subsequent module, where it is concatenated with new features. These combined features are optimized simultaneously for both the synoptic-scale and focused-scale central regions. Given that the satellite observation resolution is standardized at 4 km, we develop three modules with scales of 12 km, 8 km, and 4 km. It enables to mimic the nesting approach from weather research and forecasting model, embedding a high-resolution model within a large, lower-resolution model to capture fine resolution features (e.g., Richardson et al. (2007)). The main task, which is directly connected to Module 3, extracts the final TC center estimation results of this model. To verify the efficiency of MFT-TC, the single-CNN-based TC center estimation model, which has been widely used in previous studies, was tested. The single-CNN architecture contains four convolutional modules with two fully connected layers. Through the trial-and-error approach proposed by Wang et al. (2024), the most optimized single-CNN-based model to our dataset was utilized to verify the feasibility of our proposed models (Table 1).

Table 1
Single convolutional neural networks-based tropical cyclone estimation models, which were used as control models in this study. C, BN, P, and FC indicate a convolutional layer, batch normalization, pooling layer, and fully connected layer, independently. The numbers in each abbreviation means that C (number of kernels)@(size of the kernel), P (size of pooling layer), FC(number of kernels in the fully connected layer).

Model	Architecture
Single-CNN-based TC center estimation model	C16@7, BN, P2, dropout = 0.4, C32@5, BN, P2, C64@3, BN, P3, C192@3, C512@1, FC192, FC64

Table 2
Architecture of multi-task feature transfer deep learning-based TC center estimation model. The numbers in each abbreviation mean that number of kernels in C, size of the kernel in @, size of pooling layer in P, number of kernels in the fully connected layer in FC, and ⊙ indicates a concatenation. The bolded stages in each module were utilized for integration into sub-modules to transfer features. The upper script part represents the cropping ratio for concatenating with sub-modules.

Modules	Architecture	Output
Module 1	^{1}C16@7, ^{1}P2, ^{1}drop out = 0.25, ^{1}**C32@5**, ^{1}P2, ^{1}C64@3, ^{1}P2, ^{1}C192@3, ^{1}P2, ^{1}C512@1, ^{1}Flatten, ^{1}FC192, ^{1}FC64	Sub task 1
Module 2	^{2}C16@7, ^{2}P2, ^{2}drop out = 0.25, ^{2}C32@5, ^{1}**C32@5** $^{\mathbf{p0.75}}\odot$ ^{2}**P2**, ^{2}C64@3, ^{2}P2, ^{2}C512@1, ^{2}Flatten, ^{2}FC192, ^{2}FC64	Sub task 2
Module 3	^{3}C116@7, ^{3}P2, ^{3}drop out = 0.25, ^{3}C32@5, ^{3}P2, ^{3}C64@3, **[**^{1}**C32@5**$^{\mathbf{part0.75}}\odot$ ^{2}**P2]** $^{\mathbf{part0.5}}\odot$ ^{3}**P2**, ^{3}C192@3, ^{3}C512@1, ^{3}DR0.25, ^{3}Flatten, ^{3}FC192, ^{3}FC64	Main task

3.5. Evaluation

To evaluate the performance of TC center estimation models, distance error (DE, km) and mean DE (MDE, km) are used. Additionally, skill score (SS) is utilized for verifying feasibility of proposed model.

$$Distance\ error\ (DE_i) = distance(y_i, \hat{y}_i) \tag{1}$$

$$Maen\ distance\ error\ (MDE) = \frac{\sum_i^N (DE_i)}{N} \tag{2}$$

$$Skill\ socre\ (SS) = \frac{MDE_{proposed} - MDE_{ctrl}}{MDE_{ctrl}} \tag{3}$$

where y_i and $\hat{y}_i$ are the reference center and estimated center locations,

Table 3
Tropical cyclone intensity categories based on the Saffir-Simpson category. It is utilized for evaluating the scheme-wised multi-task feature transfer deep learning-based tropical cyclone center estimation model.

Category	Intensity (kts)
Tropical Depression (TD)	20–34
Tropical Storm (TS)	35–63
Category 1 (C1)	64–82
Category 2 (C2)	83–95
Category 3 (C3)	96–113
Category 4 (C4)	114–135
Category 5 (C5)	>135

Table 4
Scheme-wise categorical mean distance error (MDE) and skill score (SS) of scheme 2. Scheme 1 and scheme 2 indicate the MFT–TC-based center estimation approach utililzing divided training samples by eye detection algorithm (MFT-TC-div) and whole training samples (MFT-TC-whl).

Category	Sample size	MDE (km)		Skill score (%) of scheme 2
		Scheme 1 (MFT–TC-div)	Scheme 2 (MFT–TC-whl)	
TD	303	55.41	56.31	1.60
TS	406	40.49	46.24	12.43
Category 1	139	25.70	31.39	18.13
Category 2	86	19.33	23.98	19.39
Category 3	46	14.51	20.46	29.08
Category 4	54	9.93	13.55	26.72
Category 5	29	7.04	10.84	35.06
Overall	1 093	27.44	31.94	14.09

$distance(y_i, \hat{y}_i)$ indicates the distance between the reference and estimated centers, N indicates the number of test samples, and $MDE_{proposed}$ and MDE_{ctrl} represents the MDE performance of proposed model and control model, respectively.

To verify the feasibility of sample distribution method and MFT-based model, we conduct two steps of evaluation. First, two schemes according to sample divided method (i.e., Scheme 1 and *2*) were evaluated according to the intensity: Scheme 1, which divides the datasets based on the absence and presence of TC eye, Scheme 2, which uses the entire combined dataset. Subsequently, based on the optimized scheme, the performance of MFT-TC is evaluated compared to the single CNN-based TC center estimation models, which widely utilized in previous studies (e.g., Wang et al., 2024; Ho et al., 2024). In this study, the scheme-wise performance is evaluated not only for the overall performance but also for the categorical performance based on the Saffir-Simpson criteria (Table 3).

4. Results and discussion

4.1. Performance of MFT-TC according to the presence and absence of TC eye

The quantitative evaluation of the MFT–TC utilized two test sets (TCs in 2019 extracted from COMS MI and TCs in 2021 extracted from GK2A AMI). As TCs have structural characteristics that depend on their intensity, two schemes (i.e., training divided samples according to whether the TC contains eyes or not (scheme 1, MFT–TC-div) and using whole TC datasets (scheme 2, MFT–TC-whl) were tested. Table 4 presents a comparison of the performance of the two schemes using the MDE, and SS of scheme 2 as the key evaluation metrics. Overall, scheme 2 shows better performance compared to scheme 1, with SS of 14.09 %. In particular, scheme 2 outperforms scheme 1 across all categories, from TD to category 5 TC, with the skill scores improving as the TC category increases. The most notable improvement is observed in Category 5, with an SS improvement of 35.06 %. This implies that classifying the samples into those with and without the TC eye and then training them separately is highly beneficial in detecting center of strong TCs.

4.2. Performance of the multi-task feature transfer deep learning-based TC center detection

After verifying the efficiency of Scheme 1, the performance of MFT-TC is evaluated in terms of both detection performance and computing cost through comparing with widely used single CNN-based TC center estimation approach. Fig. 5 illustrates the MDEs based on their intensities. As the TC intensifies, the general center determination performance improves linearly. Notably, MFT-based TC detection consistently maintained lower errors than the single-CNN-based approaches. Especially in the moderate intensity range (55–80 knots) without TC eyes, significant improvements are noted in MFT–TC-based TC center detection, with improvements ranging from 12 % to 39 %. Previous studies have indicated that because of the structural ambiguity of unorganized TCs, it is difficult to specify TC using normal visual inspection analysis (Chaurasia et al., 2010; Zheng et al., 2019; Shin et al., 2022). To mitigate this limitation, it is necessary to propose a novel

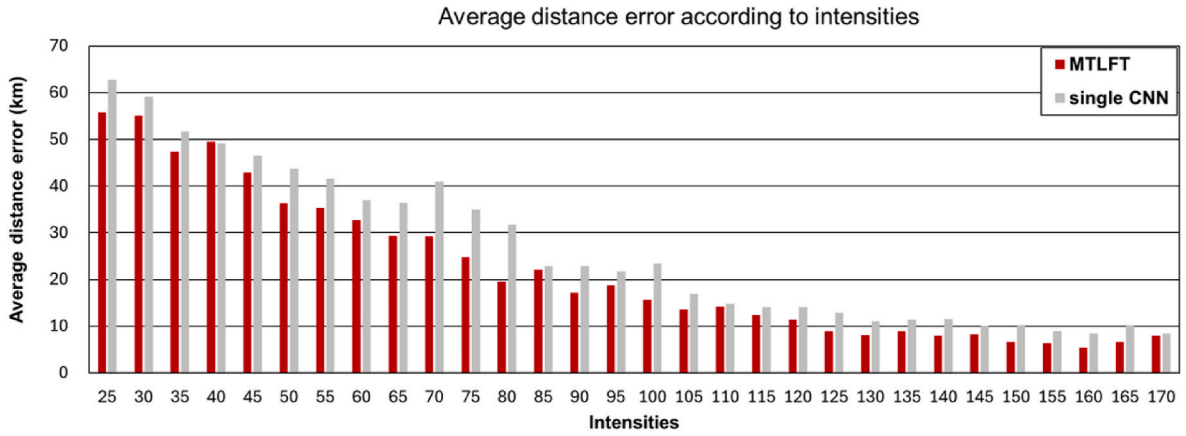

Fig. 5. Mean distance error according to intensities of multi-task feature transfer deep learning-based tropical cyclone center estimation model (MFT–TC) and single convolutional neural networks (single-CNN)-based center estimation model. Red and gray bars indicate intensity-wised mean distance error of MFT–TC and single-CNN-based estimation results, respectively.

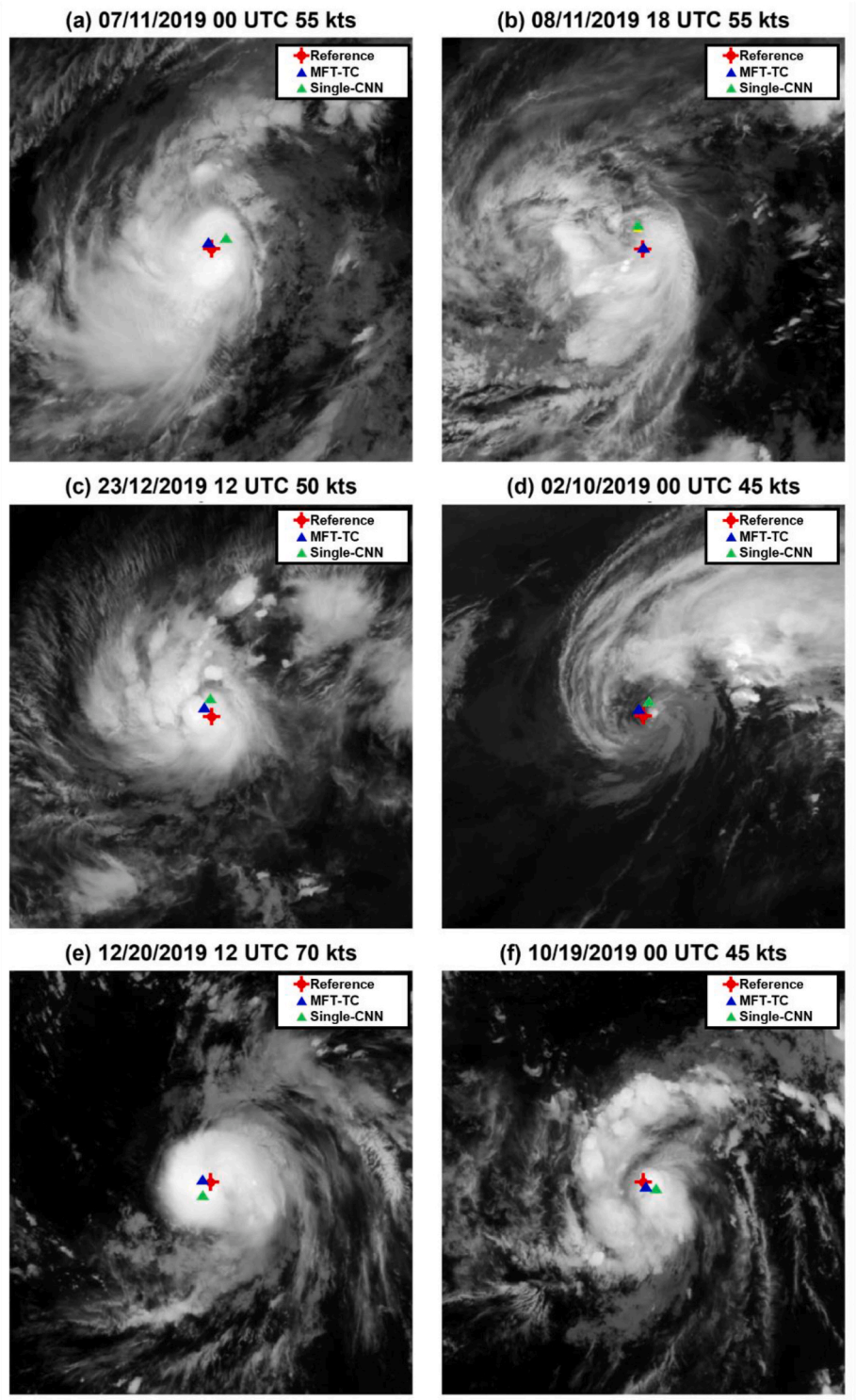

Fig. 6. Examples comparing Mult-task feature transfer deep learning (MFT) and single convolutional neural networks (Single-CNN, *Control 1*)-based TC center detection results. Red circle indicates the reference TC center location by the joint typhoon warning center (JTWC) best track. Blue and Yellow triangles indicate MFT-TC and single-CNN-based TC center detection results, respectively. The corresponding date, time (UTC), and the wind speed in knots are annotated on each subfigure.

approach for efficiently estimating the TC center location. At this point of view, proposed model significantly captures the large-scale rough pattern of the TC, which is related to center detection, and the feature information was successfully transferred to the bottom module. Fig. 6 depicts the center-detection performance, particularly for TCs without eyes. When the eye of the TC is absent, center determination inevitably relies on spiral structural characteristics. Therefore, it is difficult to determine the center location. When using the single-CNN-based TC center estimation, the model mainly focuses on the global cyclonic pattern to estimate TC center location. On the other hand, the hierarchical structure of the MFT-TC model enables the capture of both the general outflow pattern of TCs and the sequential transition to

Table 5
Comparison of previous studies and the current method for tropical cyclone center estimation. 1° of latitude and longitude correspond 111.32 km and cos (latitude)*111.32 km, respectively.

Proposed study	Method	Dataset	Spatial resolution	Evaluation target	MAE
Wang et al. (2020)	CNN	Himawari-8	2 km	2008 to 2011 and 2017 to 2019	Longitude 0.237° and Latitude 0.237°
Zheng et al. (2019)	Cloud-derived wind motion			3 TC cases	41 km
Shin et al. (2022)	Fitting TC spiral band	COMS	4 km	2019 TCs	0.38°
Wang et al. (2021)	CNN	Himawari-8	2 km		39.1 km
Wang et al. (2024)	CNN	Himawari-8	2 km	Randomly separated TCs from 2015 to 2018	29.3 km
Control using single CNN	CNN	COMS and GK2A	4 km	2019 and 2021 TCs	32.08 km
Proposed (scheme 1)	MFT-TC-div	COMS and GK2A	4 km	2019 and 2021 TCs	**27.44 km**
Proposed (scheme 2)	MFT-TC-whl	COMS and GK2A	4 km	2019 and 2021 TCs	31.94 km

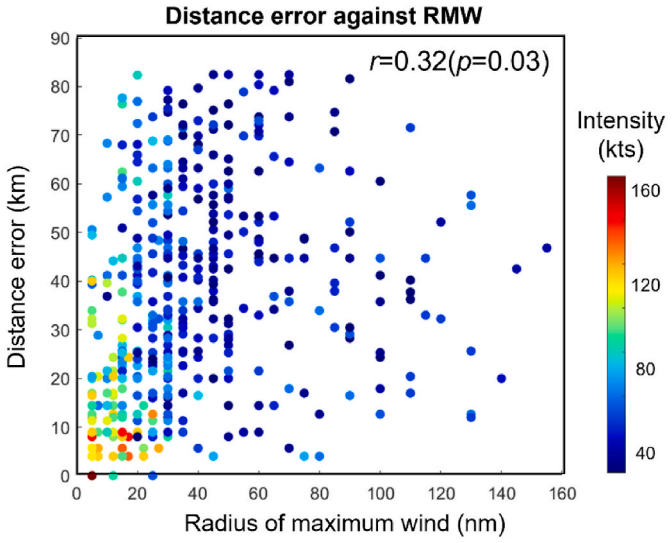

Fig. 7. Scatter plot of distance error against to the radius to the maximum wind. X-axis and Y-axis indicate the radius of maximum wind and distance error, respectively. The scatter color varies based on the intensity. R indicates the correlation from canonical crrelation analysis.

high-resolution modules, making it possible to improve center detection performance. Furthermore, the proposed model shows significant improvements in computational efficiency as well. While the single-CNN-based approach requires high dimensional input datasets which cover holistic TC regions with fine resolution, the MFT-TC works with low dimensional input datasets of varying scaled and resolutions (i.e., large-area TC images with low spatial resolution and focusing TC core regions with fine resolution). In this study, the MFT-TC method

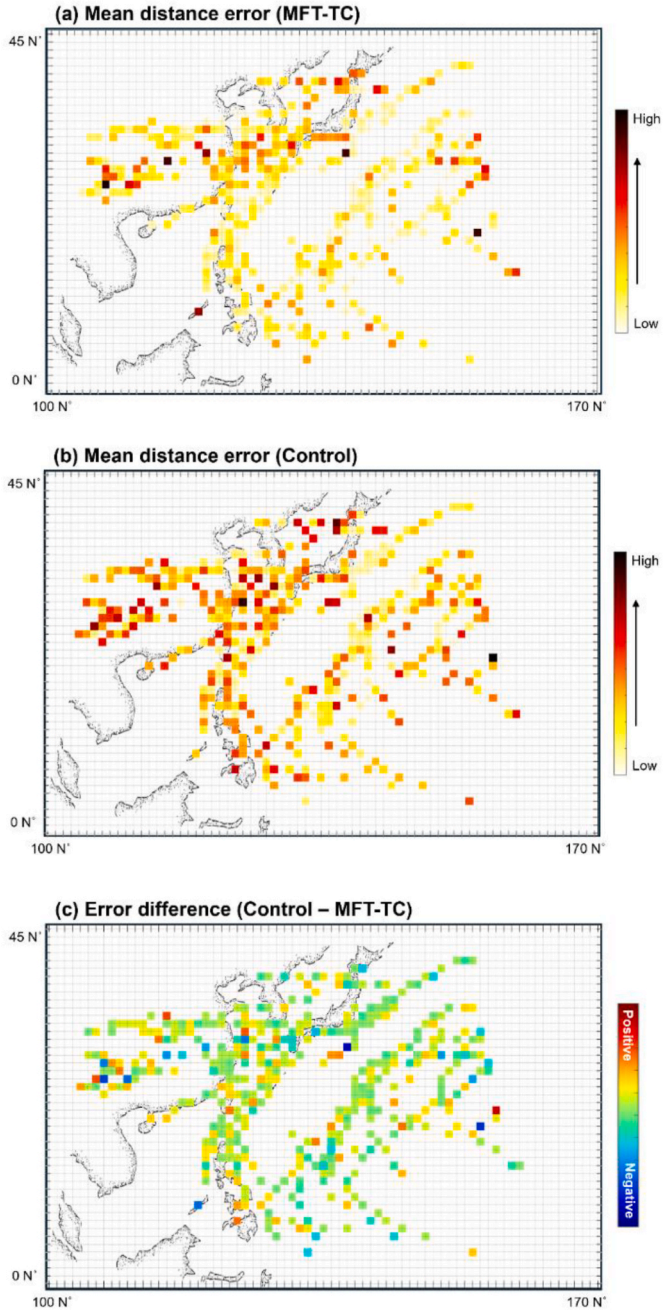

Fig. 8. The mean TC center estimation errors at each grid point of the western North Pacific for the MFT-TC (a) and the control model (b), and their differences (c).

significantly reduced the number of modeling parameters used in a single-CNN model from 43,607,698 to 22,863,290. This not only streamlined the model but also enhanced its overall computational efficiency by 47 %. Table 5 represents the performance of previous studies. While differences in validation data limit direct comparison, we can still assess the overall range of errors across studies. The results show that our method, which utilizes a 4 km spatial resolution, achieves performance comparable to or even better than other models that use a higher 2 km resolution. This suggests that our approach not only reduces computational time but also contributes to performance improvement.

The error in TC center estimation may depend not only on intensity but also on TC size, particularly the size of the TC eye. To investigate this, we analyzed the correlation between the Radius of Maximum Wind (RMW), which is closely related to TC eye size, and the TC center

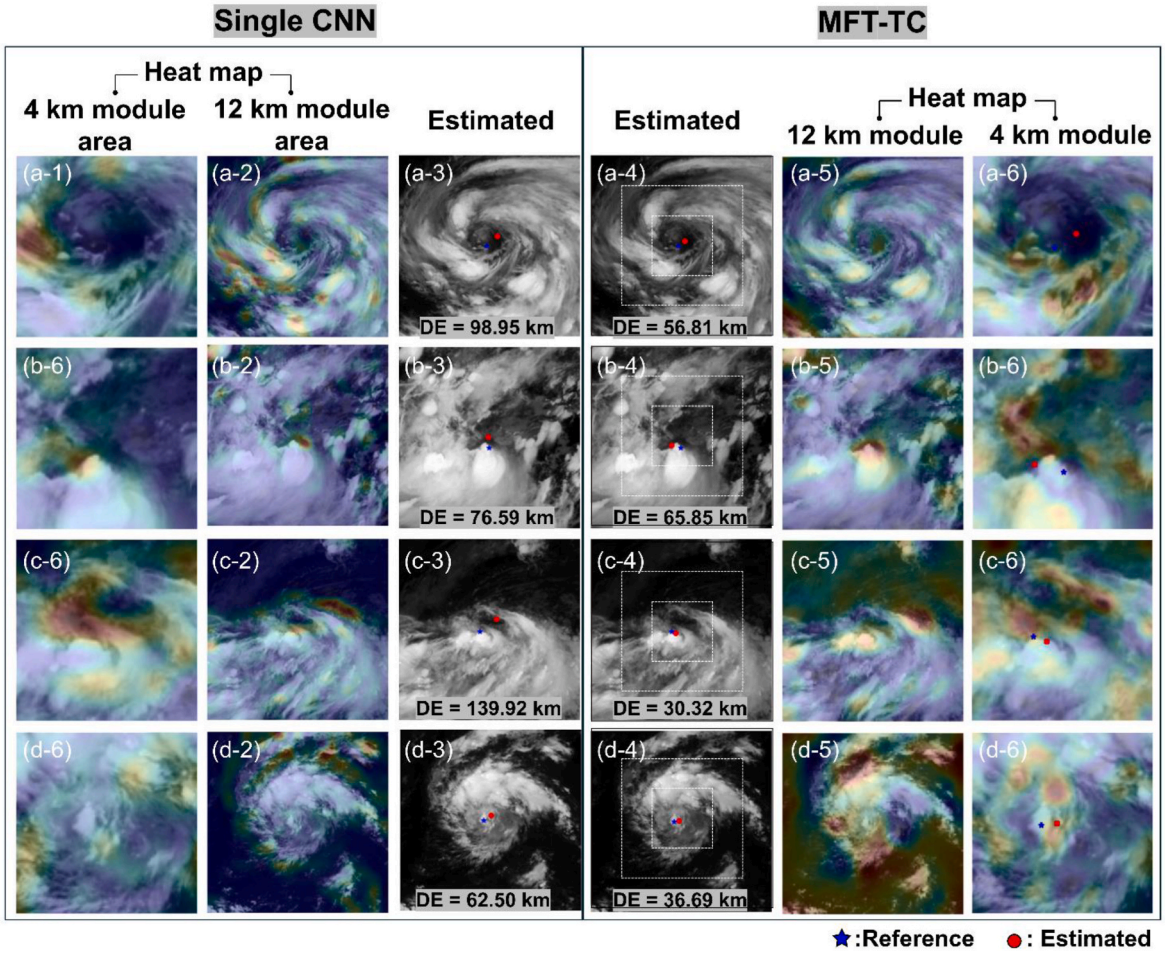

Fig. 9. Heat map-based explainability analysis of single convolutional neural networks (Single CNN)- and multi-task feature transfer deep learning model-based TC center estimation model (MFT-TC) using non-eye samples. Second and third columns (−3 and −4) indicate the estimated results from Single-CNN and MFT-TC. Red dot and blue star represent estimated and reference TC center. Distance error (DE) indicates the estimation error between Single-CNN and MFT-TC-based estimated center and reference, and DEs are shown in the third and fourth columns. While the first and second column (−1 and −2) indicates heat maps from Single CNN-based TC center estimation model over the corresponding area with 4 km and 12 km module inputs. The fifth, and sixth column (−5 and −6) imply the heat maps from 12 km to 4 km modules in MFT-TC model, respectively.

estimation error based on the MFT-TC method (Fig. 7). The results show a weak but noticeable trend of decreasing error as RMW decreases (r = 0.32, p = 0.03). This tendency is associated with the fact that lower RMW values are generally linked to stronger TCs (Li et al., 2021; Wu et al., 2021; Ruan et al., 2022). That is, as RMW decreases, TC intensity tends to increase (as shown by the color scale in Fig. 7), and strong TCs generally have lower TC center estimation errors, so the smaller the RMW, the lower the error tends to be.

Fig. 8 compares the mean TC center estimation errors between the MFT-TC and the control model at each grid point of the western North Pacific. Here, it is evident that the mean distance error is higher near the coastline. Generally, when a TC makes landfall, its energy source from the warm ocean is cut off, and increased friction with the land surface causes the TC to weaken and undergo rapid structural changes. This makes TC center estimation more challenging, ultimately leading to increased errors near the coastline. On the other hand, as a TC intensifies, its eye becomes more distinct, and its symmetry increases. This makes TC center estimation easier, leading to reducing errors (see Fig. 5). By examining the error differences between MFT and control (Fig. 8c), it can be seen that when the TC forms and develops over the open ocean and approaches land, its weak intensity and disorganized structure result in larger TC center estimation error and at these regions, the greatest error improvements occur.

4.3. Interpretation of single CNN- and MFT-based TC center estimation

In this study, the proposed model (MFT-TC) achieves a significant performance in terms of accuracy as well as computational efficiency compared to the single CNN-based model. Notably, when the samples are categorized based on the presence or absence of an eye, overall performance improved by 14.09 % (Table 4). To verify how the MFT-TC estimates are more accurate compared to the single CNN-based one, heat map visualization approach was used in this study. It is one of the visualization approaches for verifying how the CNN-based model analyzes the input dataset for extracting output (Selvaraju et al., 2017). The aggregated feature map that comes from each convolution block shows the activated region of the feature, and the last activation map is widely used for the heat map of the model. Thus, we utilized the heat map from the last convolution block for the discussion. Figs. 9 and 10 represent the visualization of single CNN and MFT-TC model trained on Scheme 1 (MFT-TC-div), which are results from the models trained using non-eye samples and eye-contained samples, respectively. When comparing in the single CNN-based heatmaps (Fig. 9 (a,b,c,d−1,2) and Fig. 10 (a,b,c,d−1,2)), the model trained with eye-contained samples tends to mostly focus on the central region while non-eye-based one tends to consider the general pattern of whole TC structure. It implies that, when the TC contained eye, it shows slightly easy to capture the central region in the raw resolution-based whole TC observations. On the other hand, when

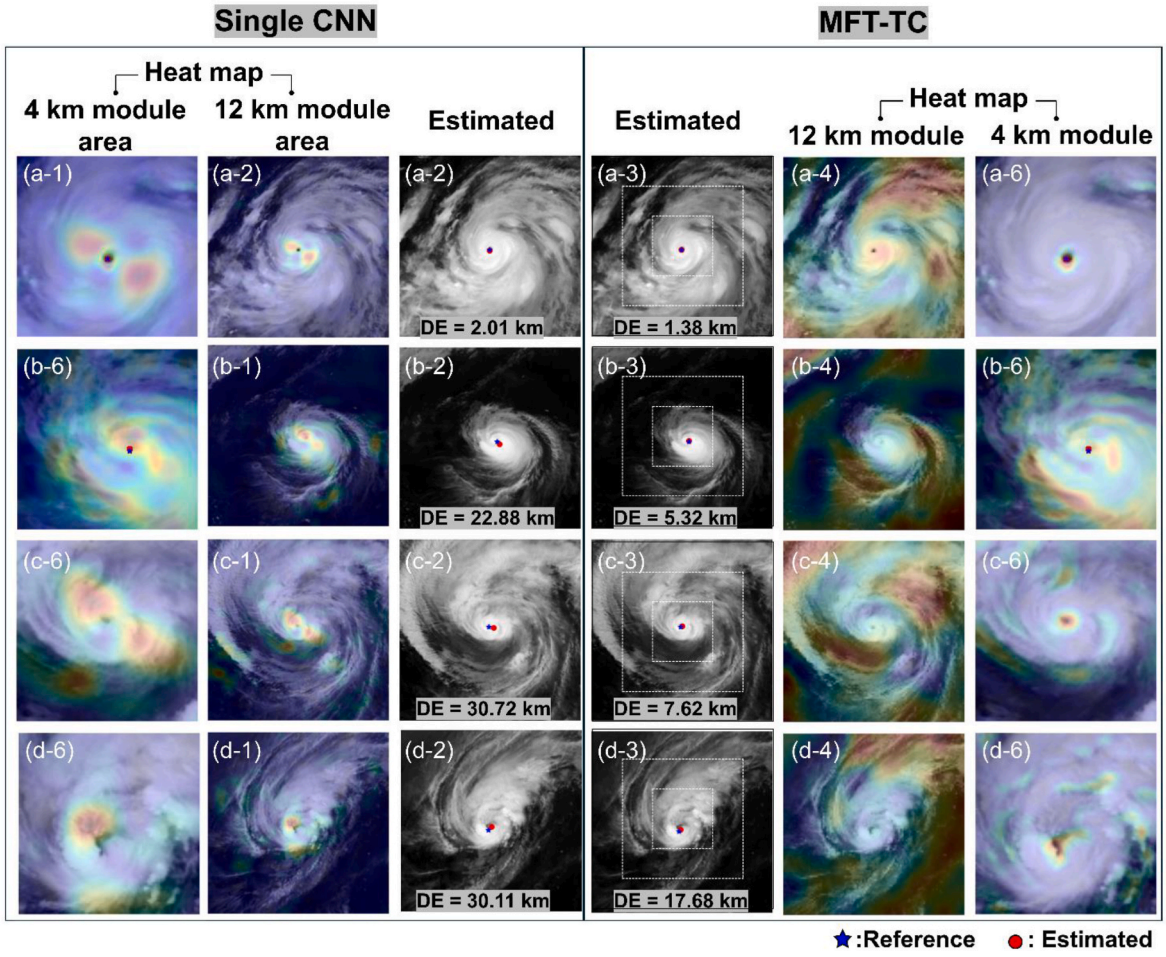

Fig. 10. Same as in Fig. 9, but using eye-contained samples.

the TC center location was estimated using MFT-TC (Fig. 9 (a,b,c,d,−5, 6) and Fig. 10 (a,b,c,d,−5, 6)), the figures show that the general TC spiral flows were well captured in the synoptic-scale module (i.e., 12 km module). As the modules become more specific, they focus increasingly on the central region (the estimated TC center).

In the case of Fig. 9 (c), since the TC is very weak with 25 kts of intensity, it is hard to generalize the region of center location; the single CNN-based estimation results showed 139.92 km of DE. On the other hand, MFT-TC achieved 30.32 km of DE in the same case. It tends to analyze the TC structure hierarchically module by module; synoptic pattern is activated in the 12 km module while spiral flow was activated in the 4 km module. In the case of Fig. 9 (d), MFT-TC performed significant improvement compared to Single-CNN-based one with considering multi-scaled pattern simultaneously in the one model. In the case of the eye-contained-based models (i.e., Fig. 10), both of single CNN and MFT-TC represents more accurate performance compared to the non-eye-based models (i.e., Fig. 10). Nevertheless, the proposed MFT-TC shows significant improvement compared to the single-CNN-based one. It also implies that the essentiality of hierarchical analyzing multi-scaled observations and supposes that the potential of MFT approach could be utilized when addressing multiple spatial and temporal scaled is necessary.

5. Conclusion

This study suggested a novel MFT-TC approach using geostationary satellite observations. By integrating feature connections across different spatial resolutions with multiple tasks, the proposed approach shows significant improvements in prediction accuracy over traditional single-CNN methods. Our results indicate that higher spatial resolution satellite images combined with feature-connected modules enhance the precision of TC center estimation and computing efficiency. Furthermore, two types of sample distribution (i.e., Scheme 1 and *2*) were validated to verify the feasibility of sample dividing according to the existence of eye or not. Through quantitative evaluation of center estimation results, scheme 1-based TC center estimation (i.e., MFT-TC-div) achieved significant improvement of 14.08 % compared to Scheme 2 (i.e., MFT-TC-whl). This result implies that it is necessary to divide the TC samples according to its structural characteristics in order to accurately determine its center. Based on the most optimized scheme (i.e., Scheme 1), performance of MFT-TC was evaluated through comparing with a single CNN-based optimized TC center estimation model, which has been widely used in previous studies. MFT-TC achieved significant skill score improvement by 39 % compared to a single CNN-based TC center estimation. Especially in the intensity range of 55–80, developing phase into a high-intensity TC and where the eye is formed, MFT-TC showed notable improvements compared to a single CNN-based model. It implies that the MFT-TC-based multi-scaled analysis contributes to the effective TC center estimation while considering rough large-scaled spiral pattern as well as specific local central region of TC with high computational efficiency (decreasing computing costs by 47 %).

Furthermore, to verify how differ the MFT-TC consider the TC observations comparing to a single CNN-based model, the heatmaps, which is one of the XAI approaches, has been utilized. These demonstrated that the MFT-TC is more effectively consider the multi-scaled morphological characteristics simultaneously, such as synoptic scaled spiral band and

specific central spatial characteristics around TC center. The proposed MFT method can be applied not only to TC-centered estimations but also to the estimation of TC structural characteristics (e.g., intensity, size). Additionally, although this technique has been applied to TCs in the western North Pacific, it can also be applied to TCs in other basins. However, since TC characteristics vary by basin (Moon et al., 2002), optimizing the model using regional TC data during the training process can further enhance its performance. By enhancing the accuracy of current TC center estimation, this study can contribute to improved TC intensity estimation. Furthermore, such advancements in initial condition estimation will ultimately aid in improving TC track and intensity forecasts.

CRediT authorship contribution statement

Juhyun Lee: Writing – review & editing, Writing – original draft, Visualization, Validation, Supervision, Resources, Methodology, Formal analysis, Data curation. **Il-Ju Moon:** Writing – review & editing, Supervision, Project administration, Conceptualization. **Jungho Im:** Writing – review & editing, Writing – original draft, Supervision. **Dong-Hoon Kim:** Data curation. **Hyeyoon Jung:** Data curation.

Declaration of competing interest

The authors declare that they have no known competing financial interests or personal relationships that could have appeared to influence the work reported in this paper.s

Acknowledgement

This research was supported by Korea Institute of Marine Science & Technology Promotion (KIMST) funded by the Ministry of Oceans and Fisheries, Korea (RS-2025-02217872) and by the National Research Foundation of Korea (NRF) grant funded by the Korea government (MSIT) (RS-2025-00560926) Jungho Im was partially supported by Institute of Information & communications Technology Planning & Evaluation (IITP) grant funded by the Korea government (MSIT) (No.RS-2020-II201336, Artificial Intelligence Graduate School Program (UNIST)). Additionally, we appreciate all editors and reviewers for their meaningful comments and valuable contributions to this paper.

Appendix A. Supplementary data

Supplementary data to this article can be found online at https://doi.org/10.1016/j.wace.2025.100796.

Data availability

Data will be made available on request.

References

Baek, Y.H., Moon, I.J., Im, J., Lee, J., 2022. A novel tropical cyclone size estimation model based on a convolutional neural network using geostationary satellite imagery. Remote Sens. 14 (2), 426.
Caruana, R., 1997. Multitask learning. Mach. Learn. 28, 41–75.
Chang, F.L., Li, Z., 2005. A near-global climatology of single-layer and overlapped clouds and their optical properties retrieved from Terra/MODIS data using a new algorithm. J. Clim. 18 (22), 4752–4771.
Chang, S., Sheng, Z., Du, H., Ge, W., Zhang, W., 2020. A channel selection method for hyperspectral atmospheric infrared sounders based on layering. Atmos. Meas. Tech. 13 (2), 629–644.
Chaurasia, S., Kishtawal, C.M., Pal, P.K., 2010. An objective method of cyclone centre determination from geostationary satellite observations. Int. J. Rem. Sens. 31 (9), 2429–2440.
Chi, J., 2022. Performance assessment of two-stream convolutional long-and short-term memory model for September Arctic Sea Ice prediction from 2001 to 2021. Korean Journal of Remote Sensing 38 (6_1), 1047–1056.
Choo, M., Kim, Y., Lee, J., Im, J., Moon, I.J., 2024. Bridging satellite missions: deep transfer learning for enhanced tropical cyclone intensity estimation. GIScience Remote Sens. 61 (1), 2325720.
Dvorak, V.F., 1975. Tropical cyclone intensity analysis and forecasting from satellite imagery. Mon. Weather Rev. 103 (5), 420–430.
Dvorak, V.F., 1984. Tropical Cyclone Intensity Analysis Using Satellite Data, 11. US Department of Commerce, National Oceanic and Atmospheric Administration, National Environmental Satellite, Data, and Information Service.
Forbis, D.C., Patricola, C.M., Bercos-Hickey, E., Gallus Jr, W.A., 2024. Mid-century climate change impacts on tornado-producing tropical cyclones. Weather Clim. Extrem. 44, 100684.
Gao, S., Zhao, P., Pan, B., Li, Y., Zhou, M., Xu, J., et al., 2018. A nowcasting model for the prediction of typhoon tracks based on a long short term memory neural network. Acta Oceanol. Sin. 37, 8–12.
Gao, M., Yu, R., Li, A., Morariu, V.I., Davis, L.S., 2018. Dynamic zoom-in network for fast object detection in large images. In: Proceedings of the IEEE Conference on Computer Vision and Pattern Recognition, pp. 6926–6935.
Hao, X., Liu, J., Heiskanen, J., Maeda, E.E., Gao, S., Li, X., 2023. A robust gap-filling method for predicting missing observations in daily black marble nighttime light data. GIScience Remote Sens. 60 (1), 2282238.
Ho, C.H., Hyeon, D., Chang, M., McFarquhar, G., Won, S.H., 2024. Geostationary satellite–derived positioning of a tropical cyclone center using artificial intelligence algorithms over the Western north Pacific. Bull. Am. Meteorol. Soc. 105 (3), E486–E500.
Hochreiter, S., 1997. Long short-term memory. Neural Computation MIT-Press.
Hu, Y., Zou, X., 2021. Tropical cyclone center positioning using single channel microwave satellite observations of brightness temperature. Remote Sens. 13 (13), 2466.
Jung, H., Baek, Y.H., Moon, I.J., Lee, J., Sohn, E.H., 2024. Tropical cyclone intensity estimation through convolutional neural network transfer learning using two geostationary satellite datasets. Front. Earth Sci. 11, 1285138.
Jung, S., Kim, Y.J., Park, S., Im, J., 2020. Prediction of sea surface temperature and detection of ocean heat wave in the South Sea of Korea using time-series deep-learning approaches. Korean Journal of Remote Sensing 36 (5_3), 1077–1093.
Knapp, K.R., Kruk, M.C., Levinson, D.H., Diamond, H.J., Neumann, C.J., 2010. The international best track archive for climate stewardship (IBTrACS) unifying tropical cyclone data. Bull. Am. Meteorol. Soc. 91 (3), 363–376.
Kurniawan, A., Khakhim, N., Wicaksono, P., 2024. Seasonal variation influence to water image properties to retrieve nearshore bathymetry based on cloud machine learning approach. Int. J. Geoinf. 20 (7), 77–99.
Lee, J., Im, J., Cha, D.H., Park, H., Sim, S., 2019. Tropical cyclone intensity estimation using multi-dimensional convolutional neural networks from geostationary satellite data. Remote Sens. 12 (1), 108.
Lee, J., Kim, M., Im, J., Han, H., Han, D., 2021. Pre-trained feature aggregated deep learning-based monitoring of overshooting tops using multi-spectral channels of GeoKompsat-2A advanced meteorological imagery. GIScience & Remote Sensing 58 (7), 1052–1071.
Lee, Y., Min, S., Yoon, J., Ha, J., Jeong, S., Ryu, S., Ahn, M.H., 2025. Application of deep learning in cloud cover prediction using geostationary satellite images. GIScience & Remote Sensing 62 (1), 2440506.
Lee, J., Yoo, C., Im, J., Shin, Y., Cho, D., 2020. Multi-task learning based tropical cyclone intensity monitoring and forecasting through fusion of geostationary satellite data and numerical forecasting model output. Korean journal of remote sensing 36 (5_3), 1037–1051.
Li, Y., Wang, Y., Lin, Y., Wang, X., 2021. Why does rapid contraction of the radius of maximum wind precede rapid intensification in tropical cyclones? J. Atmos. Sci. 78 (11), 3441–3453.
Lian, J., Dong, P., Zhang, Y., Pan, J., 2020. A novel deep learning approach for tropical cyclone track prediction based on auto-encoder and gated recurrent unit networks. Appl. Sci. 10 (11), 3965.
Liu, B.-Y., Chen, H.-X., Huang, Z., Liu, X., Yang, Y.-Z., 2021. Zoominnet: a novel small object detector in drone images with cross-scale knowledge distillation. Remote Sens. 13 (6), 1198.
Liu, T., Chen, Y., Chen, S., Li, W., Zhang, A., 2023. Mechanisms of the transport height of water vapor by tropical cyclones on heavy rainfall. Weather Clim. Extrem. 41, 100587.
Lu, X., Yu, H., Yang, X., Li, X., Tang, J., 2019. A new technique for automatically locating the center of tropical cyclones with multi-band cloud imagery. Front. Earth Sci. 13, 836–847.
Magee, A.D., Verdon-Kidd, D.C., Kiem, A.S., 2016. An intercomparison of tropical cyclone best-track products for the southwest Pacific. Nat. Hazards Earth Syst. Sci. 16 (6), 1431–1447.
Mahapatra, B., Walia, M., Saggurti, N., 2018. Extreme weather events induced deaths in India 2001–2014: trends and differentials by region, sex and age group. Weather Clim. Extrem. 21, 110–116.
Moon, I.-J., Knutson, T.R., Kim, H.-J., Babanin, A.V., Jeong, J.-Y., 2022. Why do eastern north Pacific hurricanes intensify more and faster than their western-counterpart typhoons with less ocean energy? Bull. Am. Meteorol. Soc. 103 (11), 2604–2627. https://doi.org/10.1175/BAMS-D-21-0131.1.
Richardson, M.I., Toigo, A.D., Newman, C.E., 2007. PlanetWRF: a general purpose, local to global numerical model for planetary atmospheric and climate dynamics. J. Geophys. Res.: Planets 112 (E9).
Ruan, Z., Wu, Q., 2022. Relationship between size and intensity in north Atlantic tropical cyclones with steady radii of maximum wind. Geophys. Res. Lett. 49 (3), e2021GL095632.

Selvaraju, R.R., Cogswell, M., Das, A., Vedantam, R., Parikh, D., Batra, D., 2017. Grad-cam: visual explanations from deep networks via gradient-based localization. In: Proceedings of the IEEE International Conference on Computer Vision, pp. 618–626.
Shin, Y., Lee, J., Im, J., Sim, S., 2022. An advanced operational approach for tropical cyclone center estimation using geostationary-satellite-based water vapor and infrared channels. Remote Sens. 14 (19), 4800.
Tsukada, T., Horinouchi, T., 2023. Strong relationship between eye radius and radius of maximum wind of tropical cyclones. Mon. Weather Rev. 151 (2), 569–588.
Velden, C.S., Olander, T.L., Zehr, R.M., 1998. Development of an objective scheme to estimate tropical cyclone intensity from digital geostationary satellite infrared imagery. Weather Forecast. 13 (1), 172–186.
Wang, P., Wang, P., Wang, C., Yuan, Y., Wang, D., 2020. A center location algorithm for tropical cyclone in satellite infrared images. IEEE Journal of Selected Topics in Applied Earth Observations and Remote Sensing 13, 2161–2172.
Wang, H., Xu, Q., Yin, X., Cheng, Y., 2024. Determination of low-intensity tropical cyclone centers in geostationary satellite images using a physics-enhanced deep-learning model. IEEE Trans. Geosci. Rem. Sens.
Wu, J., Kawamura, R., Mochizuki, T., Kawano, T., 2024. Increasing WNP tropical cyclone-related extreme precipitation over east Asia during boreal summer associated with PDO shift. Weather Clim. Extrem. 45, 100714.
Wu, Q., Ruan, Z., 2021. Rapid contraction of the radius of maximum tangential wind and rapid intensification of a tropical cyclone. J. Geophys. Res. Atmos. 126 (3), e2020JD033681.
Wang, C., Zheng, G., Li, X., Xu, Q., Liu, B., Zhang, J., 2021. Tropical cyclone intensity estimation from geostationary satellite imagery using deep convolutional neural networks. IEEE Transactions on Geoscience and Remote Sensing 60, 1–16.
Wu, T., Duan, Z., 2023. A new and efficient method for tropical cyclone detection and tracking in gridded datasets. Weather Clim. Extrem. 42, 100626.
Yin, R., Han, W., Wang, H., Wang, J., 2022. Impacts of FY-4A GIIRS water vapor channels data assimilation on the forecast of "21· 7" extreme rainstorm in Henan, China with CMA-MESO. Remote Sens. 14 (22), 5710.
Yu, B., Chen, F., Wang, N., Yang, L., Yang, H., Wang, L., 2022. MSFTrans: a multi-task frequency-spatial learning transformer for building extraction from high spatial resolution remote sensing images. GIScience Remote Sens. 59 (1), 1978–1996.
Yu, Y., Si, X., Hu, C., Zhang, J., 2019. A review of recurrent neural networks: LSTM cells and network architectures. Neural Comput. 31 (7), 1235–1270.
Zhang, C.J., Zhang, L., Rui, C.M., Ma, L.M., Lu, X.Q., 2024. Tropical cyclone tracking from geostationary infrared satellite images using deep learning techniques. Int. J. Rem. Sens. 45 (18), 6324–6341.
Zhang, Y., Yang, Q., 2018. An overview of multi-task learning. Natl. Sci. Rev. 5 (1), 30–43.
Zheng, G., Liu, J., Yang, J., Li, X., 2019. Automatically locate tropical cyclone centers using top cloud motion data derived from geostationary satellite images. IEEE Trans. Geosci. Rem. Sens. 57 (12), 10175–10190.
Zhu, Y., Geiß, C., So, E., 2024. Simulating urban expansion with interpretable cycle recurrent neural networks. GIScience Remote Sens. 61 (1), 2363576.